5 Magnetic Flux Topology of 2D Point Dipoles

The previous chapter demonstrated that feature-based visualization increases the abstraction level to guide the user's attention to interesting or important parts of vector fields. In this chapter, again, topological structures are used to analyze vector fields. There are, however, several important differences between these chapters—first, the physical background changes from flow fields obtained by CFD computations to magnetic fields where no inherent flow is present. Due to this change, the attention turns to flux as opposed to flow, since important physical aspects can be observed based on the existence and the magnitude of flux. Furthermore, whereas the previous chapter visualizes unsteady vector fields, this chapter is restricted to steady fields.

Magnetic fields are a subclass of vector fields with some restrictions compared to generic vector fields. A magnetic field is divergence-free; therefore, its field lines are either closed or of infinite length. Inspired by traditional vector field topology, the goal of our approach [BSW+12] was to create a visualization of the topology of magnetic flux. However, established methods from vector field topology cannot be applied in a straightforward manner because the vector field (i.e., the magnetic flux density) may be infinite at singularity points. The most prominent example of such a singularity is the magnetic dipole, which is the central object of investigation in this chapter. Here, the focus lies on static 2D magnetic fields created by sets of dipoles. Since there are no magnetic monopoles, the first non-trivial term in any field expansion is represented by a dipole. Furthermore, elementary particles like electrons are points (without physical extent) that carry the magnetic moment of a dipole. Hence, the dipole representation is highly relevant for magnetic fields.

One natural way of visualizing a magnetic field is to use field lines. Although field lines are directed and a magnetic flux is present, there is no transport of any matter involved per se. The global structure of the magnetic flux between dipoles is of special interest, i.e., the connectivity of dipoles via magnetic field lines. Here, the fact is exploited that the topology of magnetic fields is reduced to only two types of critical points: dipoles and saddles. It will be shown that magnetic flux through two dipoles is found in a region that is always bounded by two saddles. Although similar to Morse-Smale cells, these regions are also

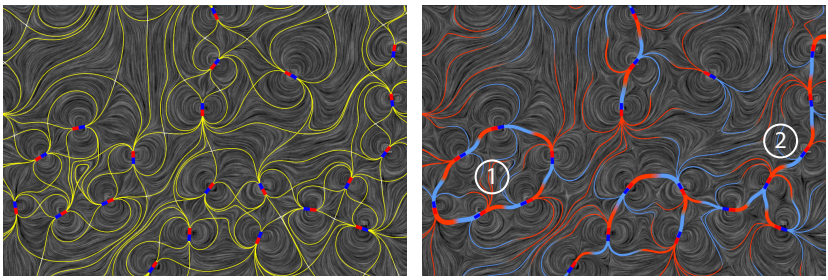

(a) (b)

Figure 5.1: Comparison of (a) traditional topology and (b) flux topology. Dipoles are represented as a two-colored rectangles with a red north pole and a blue south pole. With flux topology, magnetic rings ① or chains ② are easier to identify.

bounded by dipoles instead of sources and sinks. The interdependence of the magnetic field is utilized and its corresponding vector potential to locate these regions. The key feature presented in this chapter is the definition of distinguished field lines that connect two dipoles and are used to visualize the topology of magnetic flux. This *flux topology* is based on a new topological construct called *dipole connectrix*, or shorter connectrix. Given the task of finding dipoles that interact with each other, e.g., are forming rings or chains of magnetic flux, it is of course possible to use traditional topology. However, to accomplish this, the user has to keep track of several topological curves at once. By using connectrices, this task is reduced to following a single line. A comparison of traditional vector field topology and flux topology is given in Figure 5.1.

As an application of this visualization technique, results from the simulation of systems of single domain magnetic nanoparticles are presented. The simplest example of such a system to which this visualization has great potential is a magnetic fluid, consisting of magnetic particles with an average size of 7–9 nm, suspended in a non-magnetic carrier liquid. Recent experiments [KDK+06] have shown how complex the microstructure of two-dimensional layers of a ferrofluid can be. Additional insight into these systems was obtained in theory and by computer simulation [KCH08, PDKH09]. However, none of these approaches can directly characterize the field distribution in the sample.

Another possibility is to blend magnetic and elastic properties within a single material, by embedding magnetic nanoparticles into an elastic polymer matrix. Materials that are designed as such are called magnetic gels, or ferrogels, and can serve as the basis for various potential applications, ranging from artificial muscles, actuators, and micro machines to biomimetic energy-transducing

devices. A manifestation of magneto-elastic coupling can be observed in the deformation of a macroscopic ferrogel body in a uniform or gradient magnetic field [Zri00, RDT+10]. However, any application of these materials is based on the profound knowledge of their microstructure and on the ability to control and design them on various levels. There are only few theories that can treat the gel on the mesoscopic level, e.g., the work by Stolbov et al. [SRB11] and references therein, and simulations [WC11] aimed at the understanding of the gel microstructure. That is why, here, any additional knowledge of the magnetic field is of high relevance for further development of theoretical models.

5.1 Dual Topology of Magnetic Fields

This section summarizes the physical background that is needed for this chapter. Then, the formulation of dual vector field topology is presented for the class of vector fields which is of interest. This duality is the basis for the flux topology that is introduced in Section 5.2.

5.1.1 Physics of Magnetostatics

A comprehensive introduction to magnetostatics in particular, and classical electrodynamics in general is given in the textbook by Jackson [Jac75]. In this chapter, a setting of magnetostatics is assumed, i.e., any magnetic effects that may be additionally introduced from dynamics are ignored. Such a scenario is relevant for typical setups with steady-state behavior. The key observation is that there are no magnetic monopoles (in contrast to electrostatics with its electric monopole). Therefore, magnetic dipoles serve as the main building blocks for establishing magnetic fields. A single dipole is described by its *magnetic moment*

$$\vec{m} = \frac{1}{2c} \int \vec{x}' \times \vec{J}(\vec{x}') \, \mathrm{d}^3 x' \tag{5.1}$$

with the *current distribution* $\vec{J}$ and the speed of light c.

It is common practice to use the *vector potential* $\vec{A}$ to describe the magnetic field. The term "magnetic field" is often used to refer to the *magnetic flux density* $\vec{B}$, which is related to $\vec{A}$ as follows:

$$\vec{B} = \operatorname{curl} \vec{A}.$$

Therefore, magnetism may be described using $\vec{A}$ or $\vec{B}$. In fact, many computations in physics are based on the vector potential. In particular, computations often use series expansions of the vector potential, similar to Taylor expansions of functions. The mathematical background is based on the expansion

by vector spherical harmonics [Jac75]. This kind of expansion reads for i-th component of the vector potential $\vec{A}$:

$$A_i(\vec{x}) = \frac{1}{c||\vec{x}||} \int J_i(\vec{x}') \, \mathrm{d}^3x' + \frac{1}{c||\vec{x}||^3} \int J_i(\vec{x}') \vec{x}' \, \mathrm{d}^3x' + \cdots$$

Here, $\vec{J}$ is the current distribution that gives rise to the magnetic field. If only the first term of the expansion is used, this leads to

$$\vec{A}(\vec{x}) = \frac{\vec{m} \times \vec{x}}{||\vec{x}||^3},$$

where $\vec{m}$ is the magnetic moment of a magnetic dipole (see Equation 5.1). Put differently, the expansion of $\vec{A}$ up to the first non-vanishing term yields a magnetic dipole. Therefore, dipoles are highly relevant as, at least approximated, representation of any magnetic field; the more localized the current distribution, the better the approximation.

Finally, the magnetic flux density corresponding to $\vec{A}$ of the magnetic dipole reads

$$\vec{B}(\vec{x}) = \frac{3\vec{n}(\vec{n} \cdot \vec{m}) - \vec{m}}{||\vec{x}||^3},$$

where $\vec{n} = \frac{\vec{x}}{||\vec{x}||}$.

5.1.2 Dual Vector Field Topology

First, to describe the flux topology of 2D magnetic fields, the 3D vectors $\vec{A}$ and $\vec{B}$ are reformulated for the restriction to 2D. The 2D field is assumed to be defined on the x-y plane. For this, the 3D field has to meet two requirements. First, the z-component of the flux density has to vanish everywhere, i.e., $B_z \equiv 0$. Second, $\vec{B}$ should be independent from the z-position, i.e., it should be shift-invariant along the z-direction.

These two requirements lead to the following constraints for the vector potential $\vec{A}$. First, $\vec{A}$ can be modeled as vectors that only have a z-component; their x- and y-components vanish. Second, the vector potential is independent from the z-position. With these constraints, the magnetic flux density is obtained:

$$\vec{B} = \operatorname{curl} \vec{A} = \begin{pmatrix} \frac{\partial A_z}{\partial y} \\ -\frac{\partial A_z}{\partial x} \\ 0 \end{pmatrix} \widehat{=} \begin{pmatrix} \frac{\partial A}{\partial y} \\ -\frac{\partial A}{\partial x} \end{pmatrix} = \operatorname{curl}_2 A,$$

which indeed is a 2D field. In the above equation, the vector potential is rewritten by just using its z-component, with $A_z =: A$. Furthermore, the analog of the curl operator in 2D, curl_2, was introduced. The effect of curl_2 can be expressed as

$$\vec{B} = P\,\nabla A, \quad P = \begin{pmatrix} 0 & 1 \\ -1 & 0 \end{pmatrix}.$$

Geometrically speaking, curl_2 computes the gradient of the scalar potential A and then rotates the gradient vector by $-\frac{\pi}{2}$. This geometric observation is utilized in the following construction of the magnetic flux topology. $\vec{B}$ and ∇A are dual vector fields—in this sense, the traditional topology of $\vec{B}$ can be considered as the dual of the traditional topology of ∇A.

The effect of P on the topology of the $\vec{B}$ and ∇A fields is examined to derive the relation between primal and dual topology. Since the magnetic flux density $\vec{B}$ is divergence-free, it can only contain centers and saddles (and periodic orbits, which are not of interest to us). In turn, the rotation-free ∇A field can contain only sources, sinks, and saddles. The first observation is that critical points are not affected by P, i.e., critical points of one field are found at the same location in its dual field because P does not change vector magnitude:

$$||\vec{x}|| = \sqrt{x^2 + y^2} = \sqrt{y^2 + (-x)^2} = ||P\vec{x}||.$$

The examination of the effect of P is continued with respect to centers, sources, and sinks. These topological constructs are isotropic, i.e., they are rotation-invariant. However, P converts sources with their respective vector field

$$\vec{u}(\vec{x}) = \begin{pmatrix} a & 0 \\ 0 & a \end{pmatrix} \vec{x}, \quad a > 0$$

into counter-clockwise centers with

$$\vec{u'}(\vec{x}) = P \begin{pmatrix} a & 0 \\ 0 & a \end{pmatrix} \vec{x} = \begin{pmatrix} 0 & a \\ -a & 0 \end{pmatrix} \vec{x}.$$

Changing the sign of a results in a sink that converts likewise to a clockwise center when applying P. This effect is illustrated in Figure 5.2a). As a result, dipoles in $\vec{B}$, which can be interpreted as the composition of centers of opposite orientation at infinitesimally close distance, find their counterpart as infinitesimally close pairs of a source and sink in ∇A. Finally, the effect of P is examined for saddles. To begin, it will be shown that P does not change the determinant of any matrix M:

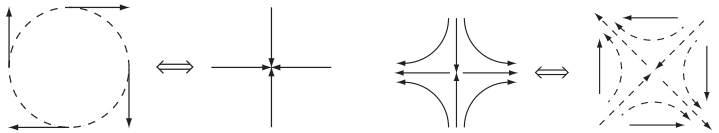

(a) (b)

Figure 5.2: (a) Centers are converted to sources or sinks (depending on their orientation) under the action of P, since every vector is rotated by $-\frac{\pi}{2}$. (b) Saddles are rotated by $-\frac{\pi}{4}$ under the action of P.

$$\det M = \det \begin{pmatrix} a & b \\ c & d \end{pmatrix} = ad - cb$$

$$\det PM = \det \begin{pmatrix} 0 & 1 \\ -1 & 0 \end{pmatrix} \begin{pmatrix} a & b \\ c & d \end{pmatrix} = -cb + ad.$$

Since $\det M$ is invariant under P, the condition for saddles of a negative determinant is not affected by P, which means that saddles in one field persist in the dual field. Now, the orientation of a saddle is considered when applying P. For the sake of simplicity, the investigation is limited to axis-aligned saddles,

$$\vec{u}(\vec{x}) = \begin{pmatrix} -a & 0 \\ 0 & b \end{pmatrix} \vec{x}, \quad a, b > 0$$

and apply P:

$$\vec{u'}(\vec{x}) = P \begin{pmatrix} -a & 0 \\ 0 & b \end{pmatrix} \vec{x} = \begin{pmatrix} 0 & b \\ a & 0 \end{pmatrix} \vec{x},$$

which results in eigenvalues $\lambda_{1,2} = \pm\sqrt{ab}$ of $\nabla\vec{u'}$.

Hence, saddles with $a = b$ of one field are rotated by $-\frac{\pi}{4}$ in the dual field, as illustrated in Figure 5.2b). For arbitrary values of a, b, the dual saddle is deformed, however, this is not of importance.

5.2 Flux Topology

In this section, the new flux topology is introduced that describes if, and how much, flux is present between dipoles.

5.2.1 Connection Regions

The discussion starts with dipoles that are oriented in opposite direction and create magnetic fields as illustrated in Figure 5.3a). There is no magnetic field

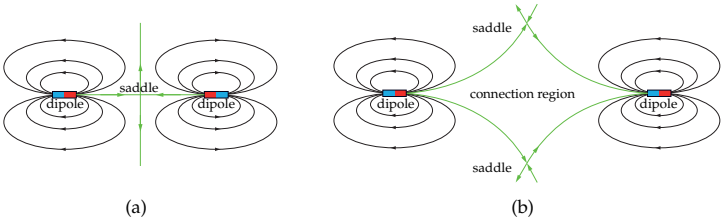

Figure 5.3: (a) In this configuration, there is no magnetic field line that connects the two dipoles. All magnetic field lines are separated by the separatrices (green). (b) Dipoles are oriented into the same direction. The region delineated by the separatrices (green) is called a dipole flux connection region.

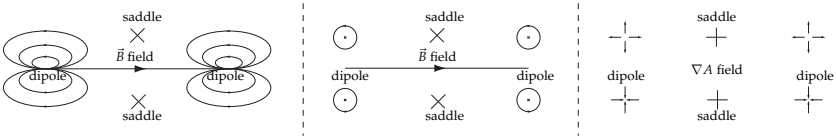

Figure 5.4: (a) Two dipoles are oriented in the same direction, which results in magnetic flux between both dipoles heading from left to right. (b) The two centers of a dipole, which are infinitly close together, are shifted apart for illustration purposes only. (c) The two centers of a dipole within $\vec{B}$ are replaced by a source and a sink in the corresponding ∇A field according to the dual topology rules.

line passing through both dipoles (the separatrices converge to the saddle in infinite time). However, of special interest is the configuration with a consistent orientation as illustrated in Figure 5.3b). Here, a region is found that consists of all magnetic field lines that connect one dipole with the other one. This region is called *dipole flux connection region*, or shorter, *connection region*. The connection region is bounded by the separatrices that start at the two saddles located between the dipoles and run through both dipoles.

The magnetic field lines around a dipole form closed curves with the centers of these curves approaching the dipole center infinitely close. If more than one dipole is involved, some of the field lines can pass through other dipoles, as illustrated in Figure 5.4. For the sake of simplicity of illustration, the infinitesimal distance between the two centers of a dipole is expanded. Every configuration of two dipoles connected by a magnetic field line can be converted into a topologically equivalent configuration as shown in Figure 5.4a)

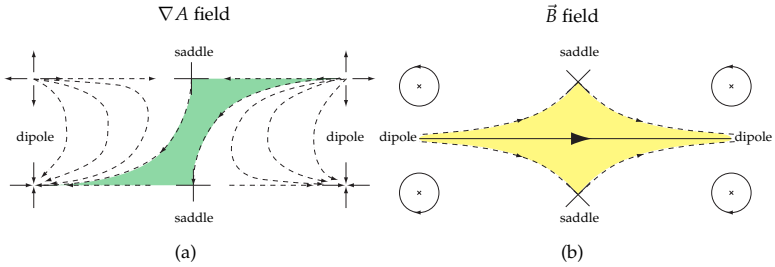

Figure 5.5: (a) A Morse-Smale cell (green) can be found in the ∇A field between connected dipoles. (b) Returning to the $\vec{B}$ field, a respective connection region (yellow) is found between the two dipoles.

and consecutively into the configuration shown in Figure 5.4b). The next step is to switch from the $\vec{B}$ field to the dual ∇A field, as shown in Figure 5.4c). As discussed in Section 5.1.2, the two centers of a dipole are now replaced by a source and a sink. In addition, the two saddles located between the dipoles are rotated (and possibly deformed).

The next step is to consider the field lines of the ∇A field, which are shown in Figure 5.5a). Please note that the source and sink pairs represent again dipoles in the ∇A field. In general, i.e., in non-degenerate cases, a Morse-Smale cell forms in ∇A between the original dipoles in $\vec{B}$. The final step in this reasoning switches back to the $\vec{B}$ field, shown in Figure 5.5b). Now, the Morse-Smale cell of the dual ∇A field converts to the previously mentioned connection region. Hence, there is always a connection region between two dipoles that share a magnetic field line. Also, such a connection region will always be defined by the two dipoles and consequently by the two corresponding saddles.

5.2.2 Connectrices

Once a connection region is found, the magnetic flux can be visualized through this region in a topological manner, i.e., its topology (connectivity of dipoles) is preserved and its morphology is neglected. To do this, a mathematical definition of connectrices is provided. To start, the set of all dipoles D is declared. A field line connecting to dipole $d_1 \in D$ either extends to infinity or connects to another dipole $d_2 \in D$, where $d_1 = d_2$ is allowed. Please note that a field line is stopped when it reaches a dipole. To proceed, F_{d_1,d_2} is defined as the set of all field lines that connect to both d_1 and d_2 and $d_1 \neq d_2$. F_{d_1,d_2} is the connection region. Now two field lines f_i, f_j are defined to be equivalent if $f_i, f_j \in F_{d_1,d_2}$.

Hence, any one field line $f_i \in F_{d_1,d_2}$ is topologically equivalent to F_{d_1,d_2}. Such a field line f is called the dipole connectrix, or shorter, connectrix of the connection region F_{d_1,d_2}.

The method that computes the visual representation of a connectrix is shown in Section 5.3.2. The magnetic flux within the connection region is visualized by the thickness of the line representation of the connectrix, and the orientation of the flux using a transition from red (north) to blue (south). The magnetic flux of such a region could be computed by integrating the magnetic flux density along any curve that connects the separatrices of the two respective saddles and stays within the connection region. As will be shown in Section 5.3.3, such an integration process can be avoided and a much simpler approach can be used to compute the magnetic flux.

5.2.3 Complete Topology

The presented method also supports domains with boundaries, e.g., limited rectangular domains that might serve as a window or come from simulations with boundaries. Within such a domain, saddle-type critical points are found using a sampling grid. The critical point extraction is the only step in this approach where a discretized version of the field is required. The remaining process can act solely on the original data given as a set of point dipoles. If a saddle is located outside of the sampling grid, it cannot be taken into account for detecting connection regions. Therefore, a connection region that would be defined by such a saddle is not found, which would lead to missing connectrices.

This problem is addressed by introducing *boundary flux indicators* that visualize where, and how much, flux crosses the borders of the data set or the boundary of the sampling grid. Boundary flux indicators are constructed as follows: to begin, boundary switch points [WTHS04] of $\vec{B}$ are located, i.e., points where $\vec{B}$ is tangential to the boundary. In this case, these points represent extrema of A along the boundary, which allows a simplified extraction by scanning the vector potential A of the outermost cells of the sampling grid. The boundary switch points serve two purposes: First, they adopt the role of saddles when extracting connection regions—they are starting points for "virtual separatrices" in $\vec{B}$, which are constructed only to delimit a connection region that would otherwise be left open (e.g., connectrix ② in Figure 5.6 would be missing). Second, they form a set S_{bsp}, whereas end points of separatrices in $\vec{B}$ that leave the sampling grid form a set S_{s}. These two sets form $S = S_{\text{s}} \cup S_{\text{bsp}}$. For two adjacent elements $e_{1,2} \in S$, a border segment is created, i.e., a segment on the boundary of the sampling grid delimited by e_1 and e_2. For each border segment, *semi-connectrices* are constructed—connectrices that are attached only to one dipole and end at their corresponding border segment. Semi-connectrix

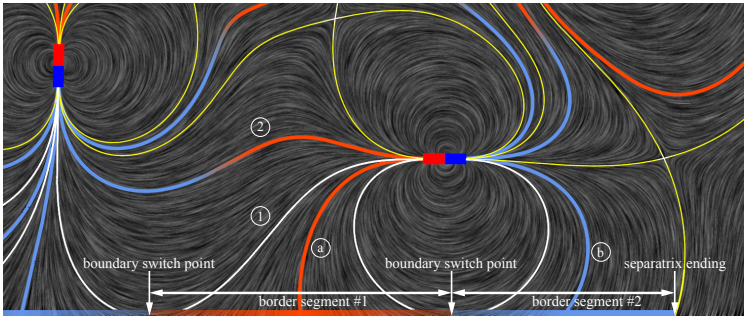

Figure 5.6: Boundary flux indicators at the bottom visualize flux affecting dipoles from the outside. Two boundary switch points and a separatrix of $\vec{B}$ form border segments #1 and #2, which in turn give rise to semi-connectrices ⓐ and ⓑ. The "virtual" separatrix ① is started at the left boundary switch point and closes the connection region represented by connectrix ②.

are colored depending on the pole of the dipole to which they connect.

As for regular connectrices, it will be shown in Section 5.3.3 that a similarly simple approach can be used to compute the corresponding flux. In addition, the border segments are visualized using boundary flux indicators: bars of fixed width that span the border segment and are of the same color as the corresponding semi-connectrix.

In total, there are three different kinds of boundary indicators depending on the type of $e \in S$ that delimits the border segment: $e_{1,2} \in S_s$, $e_1 \in S_s$ and $e_2 \in S_{bsp}$, and $e_{1,2} \in S_{bsp}$. If $e \in S_{bsp}$, gradual transparency is applied at e. This indicates that the corresponding semi-connectrix visualizes flux together with the connectrix of the adjacent connection region. If $e \in S_s$, full opacity is used instead. Figure 5.6 illustrates this situation.

5.3 Connectrix Algorithm

The algorithm that constructs connectrices is split in two parts. The first step, presented in Section 5.3.1, finds all connection regions in the data set. In the second step, one connectrix is created for each connection region (Section 5.3.2).

5.3.1 Finding Connection Regions

To find connection regions, all saddles have to be found as well as corresponding separatrices in the magnetic field. Separatrices are started at saddles and

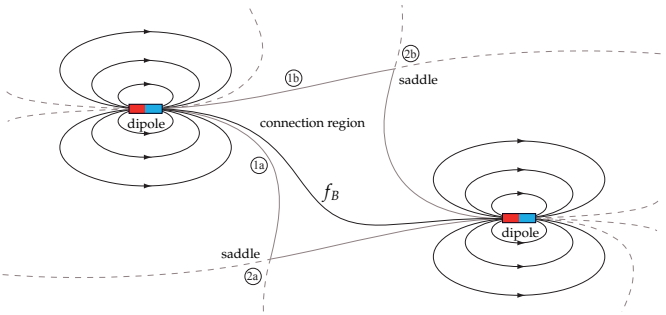

Figure 5.7: Identifying connection regions: start with neighboring separatrices (1a) and (1b) of the left dipole along with saddles at (2a) and (2b). To identify the second dipole, follow a field line f_B in $\vec{B}$ starting at the left dipole.

traced until they end at a dipole or leave the sampling grid. Depending on which pole of a dipole is hit by the separatrix, the separatrix is defined to be of type "north" or "south". Once all separatrices of the $\vec{B}$ field are created, the necessary data is at hand to identify connection regions. These regions are defined by two dipoles, two corresponding saddles, and are bounded by the separatrices that connect them as illustrated in Figure 5.3b). Separatrices ending at the first dipole have to be of opposite type (either "north" or "south") than the two separatrices ending at the second dipole. A connectrix cannot exist if the dipoles are facing each other in a topologically equivalent configuration (as shown in Figure 5.3a)). In addition, self-connectrices are not allowed, i.e., connectrices that start and end at the same dipole. This all leads to the algorithm described below.

As a preliminary step, all separatrices at a dipole that are of the same type (either "north" or "south") are sorted according to the potential A. The potential of a separatrix is obtained from the corresponding saddle position. This sorting allows one to choose "neighboring" separatrices with respect to the potential, which is essential to the algorithm.

1. For each dipole d, consider only separatrices of type "north", which form the set S_d.
2. Follow all pairs of neighboring separatrices $s_{1,2} \in S_d$; check that $s_{1,2}$ connect to different saddles.
3. Start a field line f_B in $\vec{B}$ at d between $s_{1,2}$ and trace away from d (backwards if necessary) until a dipole d' is reached.
4. A connection region is found iff $d' \neq d$.
5. Process separatrices of type "south" of d accordingly.

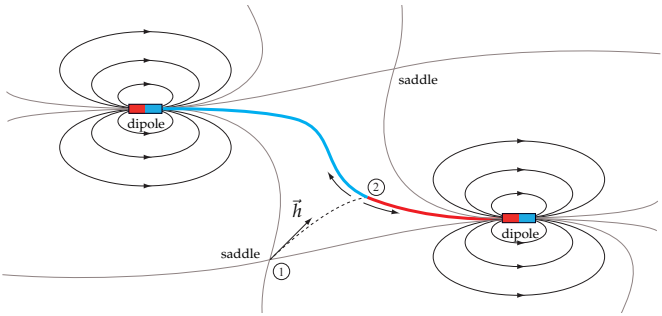

Figure 5.8: Constructing a connectrix: field line tracing is performed along ∇A into the same direction as the halfway vector $\vec{h}$ at ① until a_{avg} is found in A at ②. Tracing forwards and backwards in $\vec{B}$ constructs the connectrix for this connection region.

This algorithm is depicted in Figure 5.7 with a representative example scene. Please note that the field line $f_B$is already a valid connectrix according to the previously given definition. However, in order to create a good representation of the connectrix, additional steps are performed as described in the following section.

5.3.2 Constructing Connectrices

The second part of this method constructs a representative connectrix for each connection region. The main task is to find an appropriate seed point within this region that generates the connectrix by field line integration in $\vec{B}$ in both directions until both dipoles are reached. The idea is to choose the field line that corresponds to the mean value of the potential A of the respective connection region—in the sense of a "mean" position. The following approach was implemented to find a seed point (a special case of numerical root finding) and to construct a connectrix, as illustrated in Figure 5.8.

1. Evaluate A at the two saddle positions and compute the average a_{avg}. This represents the mean potential within the connection region.
2. Choose one of the two saddles arbitrarily and perform field line tracing in the ∇A field, heading into the connection region. Please note that this is not immediately possible, since $\nabla A = 0$ at a saddle position. Therefore, follow the half-way vector of the two separatrices that meet at the chosen saddle position. A small step is used, typically $1/10^{\text{th}}$ of the cell size of the sampling grid. Perform field line tracing in ∇A to advance

inside the connection region.

3. At each step of the tracing process in the ∇A field, access the value of A at the current tracing location. Once the value of the A field crosses the average value a_{avg}, the seed point for the connectrix is found by bisection.
4. From that point, perform forward and backward integration in $\vec{B}$ until a dipole is reached, yielding the connectrix.

In step 2, one can choose between the two saddles of the connection region as a starting point for the tracing process in the ∇A field. The resulting seed points for the connectrix are different depending on the chosen saddle; however, both seed points will be located on the same field line of the $\vec{B}$ field due to the duality of the ∇A and $\vec{B}$ fields and because of a unique a_{avg}. This is due to the fact that A is a stream function for $\vec{B}$, i.e., contours in A represent field lines in $\vec{B}$. Therefore, the final visualization for the connectrix is independent of the chosen saddle point.

5.3.3 Visualizing Magnetic Flux

In addition to encoding the topology of the flux between dipoles, the flux magnitude is visualized by varying the line width of the connectrices. This emphasizes connectrices of dipoles that create a strong magnetic flux. The magnetic flux found in a connection region is defined as the result of integrating the magnetic flux density $\vec{B}$ along any curve within this region that connects the separatrices of the two saddles. However, this integration can be avoided: it is only necessary to evaluate A at the two saddle locations. The difference of these two potentials equals the magnetic flux through the connection region. Since the potential A works analogous to a stream function, integration of flux over a curve can be replaced by a difference in the potentials of its end points.

5.3.4 Implementation

The implementation uses a uniform grid to resample the A and $\vec{B}$ field defined by the given set of dipoles. Critical points are detected according to the approach described by Helman and Hesselink [HH91]. Both separatrices and connectrices are constructed using field line integration that is performed using an adaptive step-size, fourth-order Runge-Kutta algorithm. The integration process is stopped when entering a cell that contains a dipole or when leaving the sample grid. Therefore, the sampling grid is chosen in such a way so that cells are small enough to contain at most one dipole. The prototype was implemented in C# using the XNA library on a system with an Intel Core i7 CPU running at 3.4 GHz and an NVIDIA GeForce 580 GPU. Magnetic field lines are visualized with an HLSL shader implementation of LIC [CL93].

5.4 Application

To demonstrate the usefulness of this method, it was applied to simulation and visualization problems from the domain of soft-matter sciences [KCH08]. All data sets are initially represented as collections of dipoles with varying position, orientation, and magnitude of magnetic moment. To improve the visibility of topological structures, the visualization of the magnetic field $\vec{B}$ is omitted.

5.4.1 Monolayer

In Figure 5.9, a snapshot is presented which was obtained for a ferroparticle monolayer consisting of 128 dipoles. In this case, the interparticle interaction is strong enough for the magnetic particles to form various small clusters. The prevalent topological structures in the visualization of the magnetic flux are chains and rings, readily classifying the clusters into these two groups (see, e.g., center of Figure 5.9). Moreover, this visualization gives quantitative insight in their magnetic properties, e.g., distinguished chains and loops in the visualization represent clusters with strong magnetic interaction. In this way, the technique provides a powerful approach to the analysis of ferroparticle monolayers, e.g., to differentiate between randomly aligned particles and stable clusters. This is of particular importance for understanding the microstructure of ferrofluids in confinement.

5.4.2 Ferrogel

With the series of images shown in Figure 5.10 and Figure 5.11, the time evolution spanning 1 000 time steps of a magnetic gel simulation is presented. The gel is constructed with an initially square lattice whose connectivity is indicated by black lines. The sample is composed of 4 104 dipoles and additional non-magnetic particles visualized as black dots. In this simulation, the gel is exposed to a strong external magnetic field that is aligned from left to right in the images. As the properties of the gel primarily depend on dipole–dipole interaction, this external field is omitted in the visualization.

In the first snapshot, the signature of a square lattice is still visible. Here, lattice segments that are aligned with the external field are part of chains of pronounced magnetic flux. In contrast, particles on segments perpendicular to the field are rarely part of a common connectrix. They are rather part of long, weak connectrices between neighboring lattice segments, or part of weak loop-like structures. The overall shape of the magnetic ferrogel still reflects the initial lattice because the strong horizontal chains have a repulsive effect on each other. The formation of horizontal connectrix chains proceeds during the later time steps. As these structures grow in strength of magnetic flux, the ferrogel is lo-

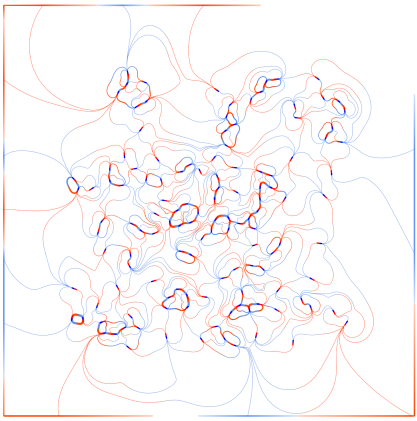

Figure 5.9: Monolayer data set. Ring and chain structures can be readily identified in the flux topology visualization. Computing the flux topology takes 14.74 seconds.

cally contracted, displacing the non-magnetic particles into saw-tooth shaped configurations. At the same time, the overall shape of the gel sample undergoes a transition into a diamond-shaped configuration, as the dipoles with energetically less advantageous configuration rearrange. In the final snapshot, the majority of the lattice segments assume a diagonal orientation, with long chains of dipoles that are co-aligned with the external magnetic field.

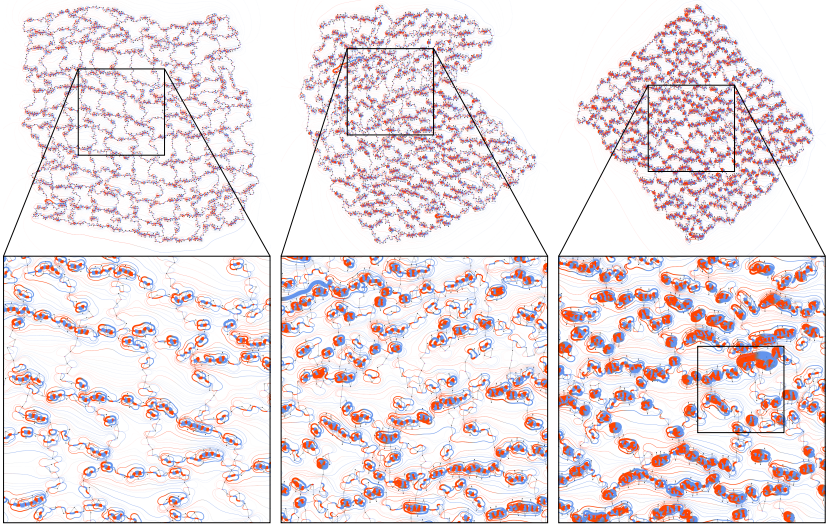

Figure 5.10: From left to right: time steps 1, 500, and 900 of a ferrogel simulation. Upper row: whole data set; lower row: zoomed-in views of the regions denoted by black rectangles. For all images, the same scaling for the flux magnitude was used. Non-magnetic particles are shown as black dots. Computing the flux topology takes 256, 270, and 264 seconds, respectively. The black rectangle in the lower right image refers to Figure 5.11.

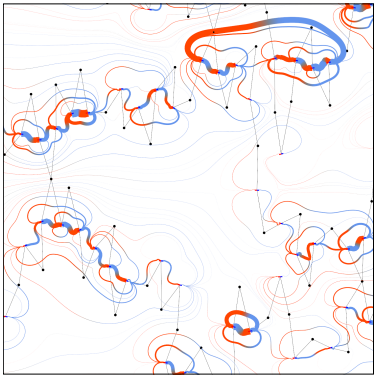

Figure 5.11: This view corresponds to the black rectangle in the lower right image of Figure 5.10. Flux is scaled down by one order of magnitude to reduce visual clutter.